
HydroGEN Seedling: Mixed Ionic Electronic Conducting Quaternary Perovskites: Materials by Design for Solar Thermochemical Hydrogen

Ellen B. Stechel
Arizona State University LightWorks
800 S Cady Mall
Tempe, AZ 85281-5402
Phone: (480)-965-1657
Email: Ellen.Stechel@ASU.edu

DOE Manager: Katie Randolph
Phone: (240) 562-1759
Email: Katie.Randolph@ee.doe.gov

Contract Number: DE-EE0008090

Subcontractor:
Princeton University, Princeton, NJ

Project Start Date: October 1, 2017
Project End Date: September 30, 2020 (project continuation after Apr 1, 2019 will be determined with a go/no-go review by DOE)

Overall Objectives

The project objective is four-fold.

- Adapt and apply first-principles computational materials design capability, to calculate and validate chemical potentials for complex off-stoichiometric redox-active mixed ionic electronic conducting perovskite metal oxides.
- Relate the calculated solid-state chemical potentials to material's thermodynamics, enthalpy and entropy of reduction, and the equilibrium off-stoichiometry.
- Relate the thermodynamics of materials to theoretical and expected water-splitting performance, noting that performance is a function of operating variables and a key driver of cost.
- Identify promising material candidates that should perform better than ceria, meet the target efficiency (solar-to-hydrogen thermal efficiency >30%), and have the potential to

approach the ultimate production cost goal of <\$2/kg H₂.

Fiscal Year (FY) 2018 Objectives

The primary objective is to develop materials' design criteria and candidate materials to co-optimize materials and the operating conditions as dictated by solar thermochemical hydrogen (STCH) reactors and system designs. The expected outcomes are to achieve the following:

- A capability for materials discovery *in silico*, based on being able to calculate solid-state chemical potentials at relevant operating conditions
- A computational capability that experiments can readily validate
- Design principles for optimal and discoverable materials
- Materials' predictions tuned to the operating conditions and/or the operating conditions tuned to a material's calculated thermodynamics.

Technical Barriers

This project addresses the following technical barrier from the Hydrogen Production section of the Fuel Cell Technologies Office Multi-Year Research, Development, and Demonstration Plan¹:

(S) High-Temperature Robust Materials.

Technical Targets

This project is focused on developing materials for solar thermochemical hydrogen production that result in technologies to produce hydrogen consistent with the following DOE technical targets:

¹ <https://www.energy.gov/eere/fuelcells/downloads/fuel-cell-technologies-office-multi-year-research-development-and-22>

- Support DOE Hydrogen and Fuel Cells
Program goals to sustainably produce hydrogen for <\$2/kg.
- Support DOE Hydrogen and Fuel Cells
Program goals to achieve 2.1×10^{-6} kg/s/m² at 1 sun (252 W/m²).
- Support DOE Hydrogen and Fuel Cells
Program goals to achieve \$1.1 million for a 1-metric-ton-per-day plant (\$790/kW).
- Support DOE Hydrogen and Fuel Cells
Program goals to achieve \$11,000 materials cost for a 1-metric-ton-per-day plant.

FY 2018 Accomplishments

- Completed benchmarking for the behavior of the strongly constrained appropriately normed (SCAN) exchange-correlation functional within the framework of density functional theory (DFT).
- Identified a U value to describe redox energetics of CeO₂-Ce₂O₃ and MnO-Mn₂O₃-MnO₂.
- Developed a novel DFT-based sub-lattice formalism for estimating theoretical Gibbs energies.
- Set up and validated thermodynamic framework with experimental data for Ce-O binary, Ce-Zr-O ternary, La-Mn-O ternary, and La-Sr-Mn-O quaternary.
- Established that the framework is extendable to other quaternaries with little modification, a major step toward representing quinary (A,A')(B,B')O perovskites.
- Developed an inverse design model for the optimal enthalpy of reduction as a function of operating conditions, including yield.
- Developed an operating design model for estimating cycle efficiency.

INTRODUCTION

The current project aims to contribute to materials discovery for improved STCH materials through fundamental quantum mechanics investigations into an exciting class of redox active, mixed ionic electronic conducting metal oxides, which can stably exist over a range of oxygen stoichiometries. By characterizing key thermodynamic properties and stability, we aim to offer strategies to boost solar-to-hydrogen thermal efficiency as well as to provide experimentalists with crucial input to synthesize, validate, and perform further testing and evaluation of promising candidates. We choose off-stoichiometric materials over phase change materials for two principal reasons. First, materials undergoing major reorganization of heavy atoms will challenge the durability criteria and will typically have kinetic limitations during reduction and/or reoxidation, whereas materials that only undergo minor ordering-disordering, structural rocking, or distortion transitions should have acceptable thermomechanical stresses and fast kinetics of reduction and reoxidation. Vacancies in the anion lattice contribute to oxygen transport moving oxygen to and from the bulk and the surface. Second, going off-stoichiometry and having disorder on the anion and cation lattices generates solid-state entropy of configurational disorder, typically absent in materials undergoing a phase transition to another crystallographic structure. High entropy structural rearrangements may exist but may not simultaneously have sufficient kinetics and/or sufficient hydrogen yield.

APPROACH

Sub-Lattice Formalism

To calculate the oxygen chemical potential within the solid phase, it is important to describe accurately the Gibbs energies of the oxidized and the reduced solid. The sub-lattice formalism, which forms the backbone of thermodynamic assessments across chemistries (i.e., CALPHAD-style calculation of phase diagrams), can be used to model the Gibbs energies.

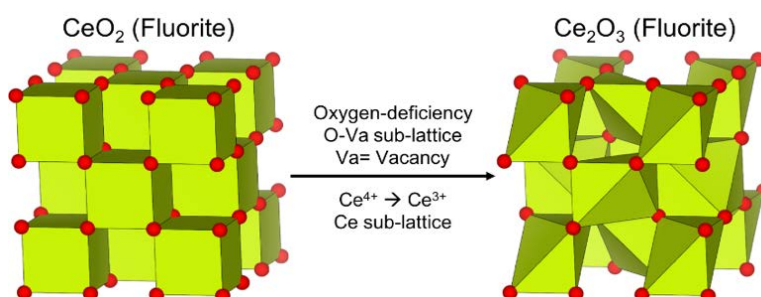


Figure 1. Illustration of the sub-lattice formalism for the fluorite phase in Ce-O binary. The structure on the left indicates stoichiometric CeO_2 while the one on the right refers to a fluorite structure with a Ce_2O_3 stoichiometry.

As an example of applying the sub-lattice formalism, consider the case of the fluorite phase of CeO_2 , which undergoes thermal reduction leading to the formation of oxygen vacancies and Ce^{3+} ions. The sub-lattice formalism described here was employed by Zinkevich et al. [1] in their thermodynamic assessment of the Ce-O binary system. Nominally, the fluorite structure has two distinct sub-lattices, Ce and O, respectively. Both sub-lattices can have two species occupying those sites, namely Ce^{3+} and Ce^{4+} in Ce sites, and oxygen (nominally O^{2-}) and vacancies in O sites. The Gibbs energy for this fluorite phase ($G_{\text{CeO}_{2-\delta}}^F$) can be written in the following functional form:

$$G_{\text{CeO}_{2-\delta}}^F = y_{\text{Ce}^{4+}} y_{\text{O}} G_{\text{Ce}^{4+}:\text{O}}^0 + y_{\text{Ce}^{3+}} y_{\text{O}} G_{\text{Ce}^{3+}:\text{O}}^0 + y_{\text{Ce}^{4+}} y_{\text{Va}} G_{\text{Ce}^{4+}:\text{Va}}^0 + y_{\text{Ce}^{3+}} y_{\text{Va}} G_{\text{Ce}^{3+}:\text{Va}}^0 + RT (y_{\text{Ce}^{4+}} \ln y_{\text{Ce}^{4+}} + y_{\text{Ce}^{3+}} \ln y_{\text{Ce}^{3+}}) + 2RT (y_{\text{O}} \ln y_{\text{O}} + y_{\text{Va}} \ln y_{\text{Va}}) + G_{\text{excess}}^F \quad (1)$$

In Equation 1, $G_{\text{Ce}^{4+}:\text{O}}^0$, $G_{\text{Ce}^{3+}:\text{O}}^0$, $G_{\text{Ce}^{4+}:\text{Va}}^0$, and $G_{\text{Ce}^{3+}:\text{Va}}^0$ are referred to as “end member” Gibbs energies with y_X corresponding to the site fraction of species X within the relevant sub-lattice. Each end member energy

corresponds to a distinct species occupancy within the fluorite structure with (i) Ce^{4+} and O occupying Ce and O sites (see left structure in Figure 1), (ii) Ce^{3+} and O occupancies (right panel in Figure 1), (iii) Ce^{4+} and oxygen vacancies within the fluorite structure, and (iv) Ce^{3+} and oxygen vacancies, respectively. Note that the Gibbs energies of non-charge-neutral structures, such as $(\text{Ce}^{4+}:\text{Va})$ and $(\text{Ce}^{3+}:\text{Va})$, are typically obtained by setting a reference state and/or using reciprocal relationships. For example, the Gibbs energy of the $(\text{Ce}^{4+}:\text{Va})$ end member is referenced to:

$$G_{\text{Ce}^{4+}:\text{Va}}^0 = G_{\text{CeO}_2} - G_{\text{O}_2}(g) \quad (2)$$

Typically, only ideal solution configurational entropy (and no other entropic contributions) is accounted for within the sub-lattice formalism. Indeed, Equation 1 has ideal-solution configurational entropy on both Ce and O sub-lattices. Finally, G_{excess}^F indicates any contributions to the Gibbs energy of the fluorite phase not captured by the end-member energies and entropy terms. Numerically, G_{excess}^F is significantly smaller as compared to the end-member and entropy contributions.

In thermodynamic assessments, experimental data (such as specific heat, enthalpy measurements, and phase transition temperatures) are used as input parameters to obtain values for the end-member and excess Gibbs energies, while the entropy term has a simpler analytical form. Here, we are calculating the relevant end-member and excess Gibbs energies entirely through DFT-based calculations, without any experimental input, and benchmark predictions that arise from a DFT-predicted model with experimental data. Specifically, we validate theoretical predictions with experimental measurements on perovskite- LaMnO_3 and SrMnO_3 .

RESULTS

Benchmarking Ternary $(\text{La,Sr})\text{MnO}_3$, 1,673K

Figure 2 displays the oxygen chemical potential profiles in $(\text{La,Sr})\text{MnO}_3$, an important candidate material for thermochemical applications, predicted by DFT+U (solid green) and from experimental data (solid red [2]). Panels a, b, c, and d of Figure 2 correspond to 10%, 20%, 30%, and 40% Sr-doping in the La sub-lattice, respectively, with all data plotted at 1,673 K (reducing conditions). Dashed green and dash-dot brown lines signify oxygen chemical potential variation in La_2O_3 and binary Mn-oxides (MnO , Mn_3O_4 , Mn_2O_3 , and MnO_2) from experimental data. Solid yellow line indicates 10 Pa oxygen partial pressure at 1,673 K. All DFT+U calculations in $(\text{La,Sr})\text{MnO}_x$ employ a SCAN+U functional with $U=2.7$ eV applied on Mn atoms only.

Importantly, the strong overlap between the solid red and solid green curves in all panels of Figure 2 indicates excellent agreement between theoretical predictions and experiments in quaternary- $(\text{La,Sr})\text{MnO}_3$, across Sr concentrations. Under oxygen partial pressures relevant for thermal reduction (solid yellow line), the measured stable compositions are $\text{Sr}_{0.1}\text{La}_{0.9}\text{MnO}_{2.988}$ (panel a), $\text{Sr}_{0.2}\text{La}_{0.8}\text{MnO}_{2.982}$ (b), $\text{Sr}_{0.3}\text{La}_{0.7}\text{MnO}_{2.978}$ (c), and $\text{Sr}_{0.4}\text{La}_{0.6}\text{MnO}_{2.974}$ (d), while theoretical predictions under identical conditions yield stable compositions of $\text{Sr}_{0.1}\text{La}_{0.9}\text{MnO}_{2.992}$, $\text{Sr}_{0.2}\text{La}_{0.8}\text{MnO}_{2.987}$, $\text{Sr}_{0.3}\text{La}_{0.7}\text{MnO}_{2.982}$, and $\text{Sr}_{0.4}\text{La}_{0.6}\text{MnO}_{2.975}$, respectively. Thus, theoretical predictions consistently slightly underestimate the experimental oxygen off-stoichiometries under Sr-substitution, with a maximum deviation of ~ 0.005 at 20% Sr-addition. Theory correctly predicts the qualitative trend of increasing O deficiency with increasing Sr content, in agreement with experiments.

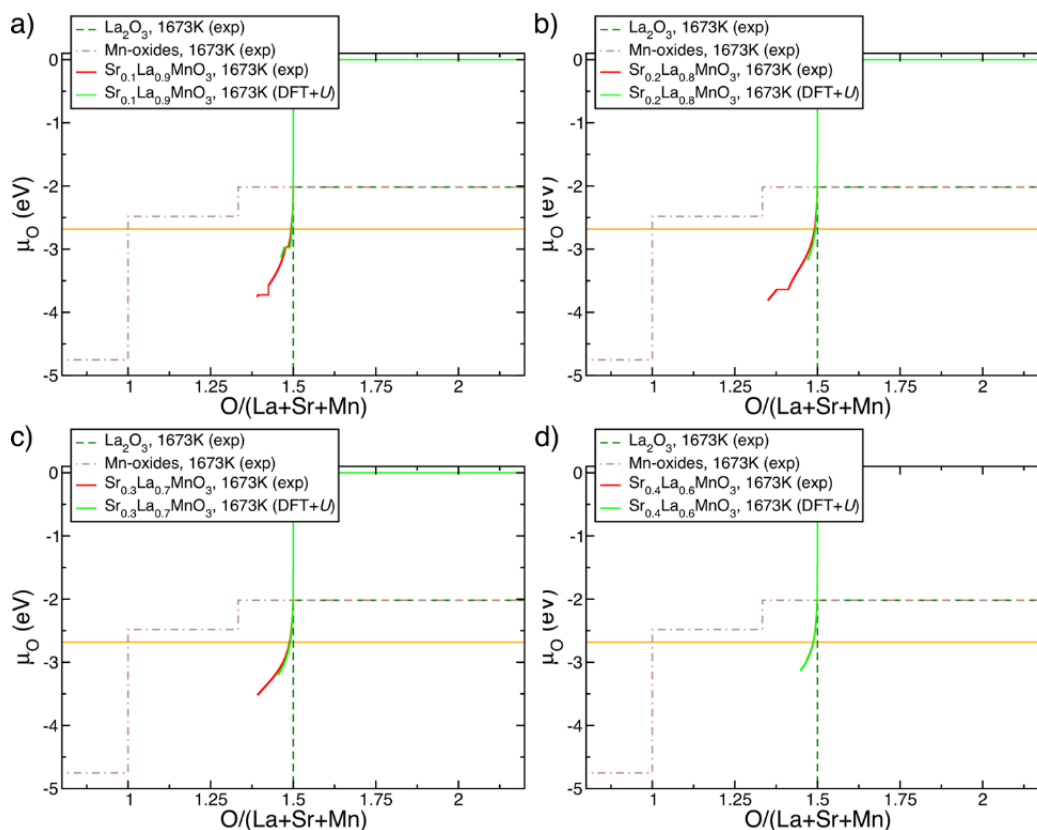


Figure 2. Comparison between experimental (red) and DFT+U-predicted (solid green) oxygen chemical potentials in perovskite-(La,Sr)MnO_x, as a function of oxygen off-stoichiometry. Dashed green and dash-dot brown lines correspond to experimental data for binary La₂O₃ and binary Mn-oxides, respectively. $U = 2.7$ eV is applied on Mn atoms during DFT+U calculations of (La,Sr)MnO_x. All data displayed here correspond to 1,673 K (temperature of thermal reduction).

Benchmarking Ternary (La,Sr)MnO₃, 873K

Figure 3 shows the oxygen chemical potential profiles in (La,Sr)MnO₃ at (a) 10%, (b) 20%, (c) 30%, and (d) 40% Sr-addition, as predicted by DFT+U (solid green) and from experimental data (solid red [2]). The solid indigo line indicates $p_{\text{H}_2\text{O}}/p_{\text{H}_2} = 9$ at 873 K, corresponding to water-splitting conditions. All DFT+U calculations add $U = 2.7$ eV on Mn atoms within a SCAN+ U framework.

Under water-splitting conditions, the theoretical calculations accurately capture the qualitative trends in oxygen off-stoichiometry, across all Sr-additions, as indicated by the strong overlap between the solid red and solid green lines in all panels of Figure 3. However, there are subtle variations between theoretical predictions and experimental observations. For example, at 10% Sr (panel a), theory predicts a significantly lower oxygen deficiency ($\text{Sr}_{0.1}\text{La}_{0.9}\text{MnO}_{2.999}$) compared to experiments ($\text{Sr}_{0.1}\text{La}_{0.9}\text{MnO}_{2.983}$). Similarly, under higher Sr additions (panels b–d, Figure 3), the perovskite phase is not expected to be thermodynamically stable under the water-splitting conditions, whereas theory predicts the perovskite to be stable with negligible oxygen deficiency. The discrepancy between theory and experiment may be due to several factors, such as La-deficiencies altering the stability of the perovskite, errors in the experimental fits to the thermodynamic Gibbs energy functions, and inaccuracies in measuring oxygen off-stoichiometry under water-splitting conditions. Note that although experimental Gibbs-energy fits indicate that the (La,Sr)MnO₃ should not be stable at >10% Sr addition under water-splitting conditions, the perovskite phase may be kinetically stable. Nevertheless, our conclusion is that our theoretical framework is robust enough, as it has been validated against ternary- and

quaternary-perovskite phases in the La-Sr-Mn-O system, and it can be further extended to quinary systems where the B-site (Mn sub-lattice) of the perovskite phase also contains substitutions.

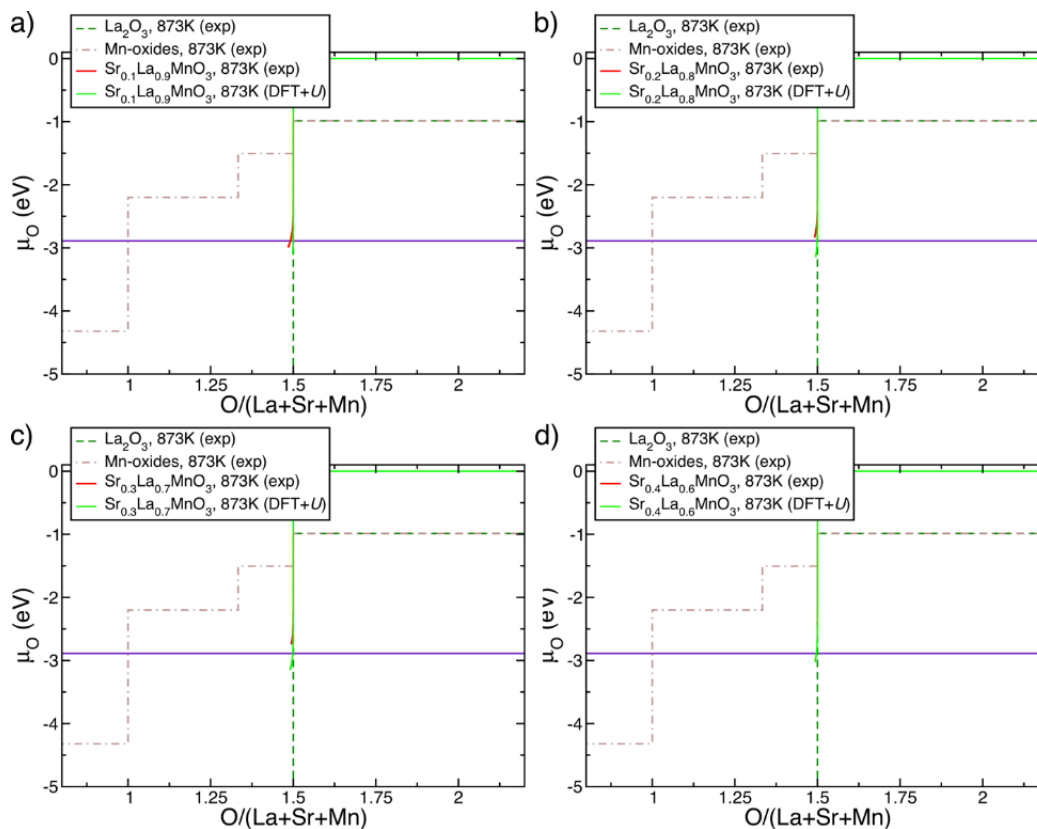


Figure 3. Comparison between experimental (red) and DFT+U-predicted (solid green) oxygen chemical potential in perovskite-(La,Sr)MnO_x, as a function of oxygen off-stoichiometry. Dashed dark green and dash-dot brown lines correspond to experimental data for binary La- and Mn-oxides, respectively. DFT+U calculations are done with $U = 2.7$ eV applied on Mn atoms. All data displayed here correspond to 873 K (temperature of water splitting).

Inverse Design

Desirable Chemical Potential Map

The benchmarking of theoretical predictions against experimental data in binary (CeO₂), ternary (La-Mn-O, Sr-Mn-O, Zr-Ce-O), and quaternary (La-Sr-Mn-O) oxides gives us confidence that the DFT-based sub-lattice formalism can act as an effective model to determine an approximate redox capacity for a given candidate material. Hence, our theoretical framework can be a refined second filter, after a high-throughput first filter based on simpler parameters such as the oxygen vacancy formation energy, to identify promising candidates for solar thermochemical applications. However, we expect to be able to identify other thermodynamic factor(s) that contribute to the oxygen off-stoichiometry of a given material, beyond the oxygen vacancy formation energy, based on the trends we observe using the sub-lattice framework, which can in turn be used to quickly screen for potential candidates.

Bayesian Inference of Thermodynamic Model Parameters

In support of this project, the principal investigator has been working closely with the Sandia National Laboratories “Uncertainty Quantification in Computational Models of Physical Systems” node principal investigator Bert Deusschere. One of the goals of the project is to predict the thermodynamic efficiency of water splitting with specified uncertainty for newly developed materials as a function of the operating

conditions. This Sandia National Laboratories node contributes to this goal by determining the confidence needed in the components that feed into that efficiency computation in order to meet the desired accuracy. The principal investigator developed the models and thermodynamic formulism.

Bayes' rule updates prior belief in parameter values (λ) with data (δ), to obtain posterior belief in the parameter values:

$$p(\lambda|d, \mathcal{M}) = \frac{p(d|\lambda, \mathcal{M})p(\lambda, \mathcal{M})}{p(d|\mathcal{M})} \quad (3)$$

We have developed four defect-free model fits of increasing complexity that allow for a relatively simple extraction of the enthalpy as well as quantifying the error in the enthalpy. The data (data can come from experiment or from computation or a combination) is assembled as a “measurement” triplet at equilibrium conditions, $\{\delta, T, pO_2\}$. We found it convenient to first convert the triplet to three transformed and unitless variables:

$$\beta = \left(\frac{T_{ref}}{T}\right) \quad (\text{temperature transform}) \quad (4a)$$

$$u \equiv \frac{1}{2} \ln\left(\frac{pO_{2,ref}}{pO_2}\right) \quad (\text{oxygen partial pressure transform}) \quad (4b)$$

$$z \equiv -\ln(\delta) \quad (\text{reduction extent transform}) \quad (4c)$$

For a defect-free model independent fit of the material relationship between $\{\delta, T, \text{ and } pO_2\}$ we use the following convenient functional form, convenient because it is easily inverted in terms of Z or in terms of u , also making it easy to determine the following:

$$z = \frac{z_{ref} + f_{10}(1-\beta) + f_{20}u + f_{30}u(1-\beta)}{1 + f_{11}(1-\beta) + f_{21}u + f_{31}u(1-\beta)} \quad (5a)$$

$$u = \frac{(z - z_{ref}) - f_{10}(1-\beta) + f_{11}z(1-\beta)}{f_{20} - f_{21}z - (f_{30} - f_{31}z)(1-\beta)} \quad (5b)$$

Model A: $f_{11} = f_{21} = f_{30} = f_{31} = 0$; Model B1: $f_{11} = f_{30} = f_{31} = 0$; Model B2: $f_{30} = f_{31} = 0$; and Model C: all parameters are active.

We infer the distribution of those parameters such that when model realizations are sampled from those random variables, they span the range of predictions due to model error [3].

In Figure 4, the shaded areas represent the mean prediction plus or minus one standard deviation, plotted in a cumulative way (i.e., the extent of the model error bars covers the cumulative effect of surrogate error, posterior uncertainty, and model error).

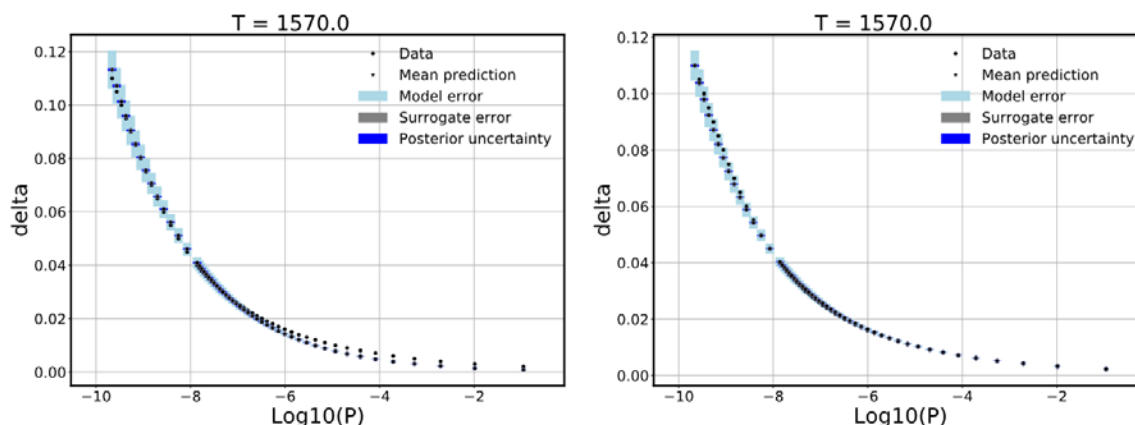


Figure 4. Model error captures the difference between data and predictions. Model error embedded in f_{10} and f_{20} for models A (left) and B1 (right). Model error is the largest contribution to predictive uncertainty. Model A: Mean parameter set is $\{z_{\text{ref}}: 14.82, f_{10}: -23.78, F_{20}: -0.4919\}$ and Model B2: Mean parameter set is $\{z_{\text{ref}}: 11.67, f_{10}: -17.37, f_{20}: -0.4384, F_{21}: -0.02567\}$.

CONCLUSIONS AND UPCOMING ACTIVITIES

The benchmarking of theoretical predictions against experimental data in binary (CeO_2), ternary (La-Mn-O , Sr-Mn-O , Zr-Ce-O), and quaternary (La-Sr-Mn-O) oxides gives us confidence that the DFT-based sub-lattice formalism can act as an effective theory and simulation model to determine an approximate redox capacity for a given candidate material. Hence, our theoretical framework can be a refined second filter, after a high-throughput first filter based on simpler parameters (e.g., the oxygen vacancy formation energy), to identify promising candidates. Moreover, we expect to be able to identify other thermodynamic factor(s) that contribute to the oxygen off-stoichiometry of a given material, beyond the oxygen vacancy formation energy, based on the trends we observe using the sub-lattice framework.

We find that the sub-lattice formalism is powerful and with quinary extensions of $(\text{La,Sr})\text{MnO}_3$ will allow for an extensive exploration of the perovskite family for candidate materials. It also permits the identification of the governing thermodynamic variables that control the oxygen deficiency of any given material, at a given temperature and oxygen partial pressure. Further characterization of uncertainty with propagation of chosen model error into thermodynamic properties will allow propagation of uncertainties into our cycle efficiency model, tying all the pieces together.

FY 2018 PUBLICATIONS/PRESENTATIONS

1. E. B. Stechel, "HydroGEN: Advanced Water Splitting Materials," Invited presentation at the International Workshop on Solar Thermochemistry, Julich, Germany, September 12–14, 2017.
2. Gopalakrishnan Sai Gautam and Emily A. Carter, "Evaluating Transition-Metal Oxides within DFT-SCAN and SCAN+U Frameworks for Solar Thermochemical Applications," *Phys. Rev. Mater.* 2 (2018): 095401.

REFERENCES

1. Matvei Zinkevich, Dejan Djurovic, and Fritz Aldinger, "Thermodynamic Modelling of the Cerium–Oxygen System," *Solid State Ionics* 177 (2006): 989.
2. A. Nicholas Grundy, Bengt Hallstedt, and Ludwig J. Gauckler, "Assessment of the La–Sr–Mn–O System," *Computer Coupling of Phase Diagrams and Thermochemistry* 28 (2004): 191–201.
3. K. Sargsyan, H.N. Najm, and R. Ghanem, R. "On the Statistical Calibration of Physical Models," *International Journal of Chemical Kinetics* 47, no. 4 (2015): 246–276.